Experimental Mechanics in Engineering and Biomechanics - Proceedings ICEM20
20th International Conference on Experimental Mechanics, Porto 2-7 July 2023
https://paginas.fe.up.pt/~icem20/proceedings_icem20/

PAPER REF: 19981

IN LINE DEFECT DETECTION IN STEEL WELDING PROCESS BY MEANS OF THERMOGRAPHY

Luca Santoro[1], Raffaella Sesana[1(*)], Rosario Molica Nardo[2], Francesca Curà[1]
[1]DIMEAS, Faculty of Engineering, Politecnico di Torino, Torino, Italy
[2]AdES Group, Palemo, Italy
[(*)]*Email:* raffaella.sesana@polito.it

ABSTRACT

In welding processes, the in-line identification of defects during manufacturing is a key aspect of a safe, reliable and economical process. Among the various non-destructive techniques, thermography is a particularly suitable technique as it is a non-contact full-field technique. However, this technique still has aspects to be improved, in particular as regards the definition of the resolution and the quantification of the extent of welding non-conformities in industrial production contexts. In the present work, an approach based on real-time defect detection on welded joints supported by its numerical model is proposed and analyzed for two arc welding processes, SMAW and GMAW on a steel alloy by means of active thermography, in order to reduce the time and costs of inspections. Different defects are identified, outlined, and discussed. Furthermore, a metallographic analysis is carried out to verify the accuracy of the model.

Keywords: welding, thermography, defect detection, NDT.

INTRODUCTION

Welded joints are commonly used as permanent mechanical connections in mechanical components. However, various factors can affect the welding properties and generate flaws, such as incorrect weld parameters, inadequate preparation and cleaning of the weld grooves. It is crucial to detect these flaws, such as pores or cracks, in order to evaluate the acceptability of the joint, as they can significantly impact the mechanical properties like fatigue life and tensile strength. There are several mechanisms that can lead to the formation of flaws in welding, as discussed in Ardika's work [1] that presents an overview of defect generation mechanism in aluminum welded joints. Filyakov's work [2] investigates the effect of arc instability on defect formation in pipe welding, and the results show a correlation between flaws and the arc interruption zone, as well as a strong relation between molten pool dynamic phenomena and anomalies in the weld bead. Similarly, the study presented by Hong [3] proposes a visual sensing algorithm applied to images of the weld bead in climbing helium arc welding process, where the melt pool solidification is found to be related to defect creation. Another study by Nguyen [4] focuses on weld pool dynamics and flaws, demonstrating that analyzing molten flows can help identify bead dimension, lack of penetration, burn trough, and humping.

Most of the flaws originate in the weld pool, such as pores and hot cracks, or in its proximity due to the various physical and chemical processes that take place. Discontinuities in the welding process introduced by factors such as an irregular arc, improper preparation of the welding groove (e.g., bad milling, contaminated surface), improper pre- and post-heat treatment, or incorrect process parameter setup, can lead to defect formation [5]. In industrial settings, non-destructive tests are typically performed at various processing steps to check the

quality of a joint, as seen in Aucott's online radiography study of hot crack formation [6]. The depth of weld penetration is closely related to the temperature of the welding pool [7]. To address this issue, [8] proposes a real-time detection method based on thermal sensing of the welding pool surface. The study investigates the correlation between the welding pool temperature and penetration for various welding currents in the tungsten arc process applied to SAE steel. A pyrometer is used to acquire point temperature in the welding pool, but positioning it correctly is crucial. A simple thermal signal processing procedure, using two filters, is implemented to detect defects above a certain threshold value. The study introduces artificial defects, such as micro-inclusions and water spraying, and detects them through perturbations in the cooling profiles' thermal contours. However, the study does not conduct a sensitivity analysis on defect size and location. Building on [8], [9] presents a study on the optimal offset distance between the IR sensor (pyrometer) and welding torch to calibrate a real-time quality detection procedure. The cooling transient's thermal response is related to welding quality, and deviations in the local temperature at different distances from the welding torch may result from non-standard welding processes. The study uses a pyrometer and does not investigate superficial or subsuperficial defects. In [10], thermographic acquisition of a single-pass plasma weld is used to correlate the weld joint's tensile strength and micro-hardness with the cooling rate for stainless steel. The cooling rate between 800 and 500°C at points on the welding line is the parameter used to correlate with tensile and hardness properties. The study assumes that the welding microstructure influences mechanical properties and is affected by the cooling process. The high-speed IR camera is used to detect points on the welding surface where the temperature is higher than in the welding pool. Regarding thermal simulation, different approaches have been explored. Some engineers prefer to simulate the joint's global thermal behavior by introducing a thermal source and fill material to predict cooling curves, microstructures, and distortions. Others opt for a more accurate analysis that considers fluid dynamics, electrical and metallurgical phenomena. In [11], a thermal measurement of a laser welding of a polymer is presented, and a COMSOL Multiphysics Software numerical thermal simulation is used to validate the thermal data.

In [12], an aluminum T-joint was studied by conducting thermographic acquisition on the surface opposite to the welded one in two different welding conditions. The acquired surface was coated with graphite to maximize thermal emission, and thermal data and micrographic images were used to calibrate a numerical finite element model in order to estimate the thermal field and compare the two welding processes. The simulation was carried out using COMSOL Multiphysics software. In [13], the simulation was conducted using the research software *Flow 3D*, which allowed for the simulation of the free flow of the droplet and weld pool moving along the weld path. This approach provided indications about the thermal behavior of the joining, especially in terms of the influence of the groove shape on the melt pool sustain and heat evacuation ability. The same approach was used in [14] for a numerical simulation of defect formation in narrow gap GMAW of 5083 Al-alloy, using *Flow 3D* software. Similarly, [15] presented an example that included an arc heat flux model, an arc pressure model, and an electromagnetic force (EMF) model. Other researchers focused on the thermal transient phenomena without considering fluid dynamic and electrical phenomena. In [16], the author used *MSC-MARC-MENTAT* software to model the welding process using a thermo-mechanical simulation that accurately calculated the thermal behavior of the joining process by using a moving thermal source. This approach was computationally lighter and easier to validate. In [16], the author showed how it was possible to predict phase fraction in multiphase material, such as steel, using thermal cooling transient simulation results and the PLOTV subroutine of MSC-MARC. Similarly, [17] performed a simulation in MSC-MARC-MENTAT to predict distortions in wire arc additive manufacturing.

An overview of thermal source models is presented in [18], with the most commonly used model for arc welding applications being the Goldak model. In [19], a simulation of a laser-MIG hybrid arc brazing-fusion welding of Al alloy to galvanized steel was presented using ANSYS software. The thermal transient induced by the two heat sources, laser beam and electric arc, was simulated and influenced by the dissimilar metals which took part in the process.

The objective of this work is to propose a procedure for subsurface defect detection by means of real-time passive thermographic analysis of the welding process of steel laminates. In particular, lack of penetration, suction pores, spatter, and burnthroughs were artificially induced in welded joints. FEA simulations of the thermal transient of the process and of the resulting microstructure and extension of the HAZ were performed, followed by experimental validation.

MATERIALS AND METHODS

This work aims to present a preliminary approach for real-time infrared monitoring of flaws in the welding process of steel joints, specifically focusing on the SMAW and GMAW processes. Two simple case studies were selected: a butt joint and a tee joint. The base material used is S275JR steel, and its chemical composition is reported in Table 1.

Table 1 - Chemical composition (%wt) of S275JR steel.

C%	Mn%	P%	S%	N%	Cu%
0.21	1.5	0.035	0.035	0.012	0.55

EXPERIMENTAL METHOD

The welding system used in this study consists of a TECNOWELD MIG 110 machine with a range of 35-100 A and a wire size of 0.6-0.8 mm, as well as an AWELCO ARC 250 machine. For the SMAW technique, the consumable used is Oerlikon TENAX 35S with a diameter of 2mm. The thermal acquisition system utilized is a Flir A40 with a 24° lens and a temperature range of 300°C to 2000 °C. The thermal data are processed with FLIR ResearchIR. Artificial flaws, such as lack of penetration, suction pores, spatter, and burnthroughs, were intentionally created by using incorrect welding parameters and/or practices. Regarding the thermal post-processing analysis, three different types of curves were monitored and processed. The first type of curve (C1) consists of heating and cooling curves (time plots) of single points positioned on the axis of the welding. The time plots were extracted from the thermal acquisition, and the selected points were represented by a 3-pixel x 3-pixel ROI in the center of the weld path. In particular, points corresponding to sound and defective areas were acquired. The second type of curve (C2) consists of the temperature profile of the entire welding line at a given time instant, which is the temperature profile along the weld path. Finally, the third type of curve (C3) is represented by the temperature profile of a line perpendicular to the weld path at the time instant corresponding to the temperature peak in the welding point for sound and defective welding areas. A micrographic analysis of the welding cross-section, using *Nital 3%* chemical etching, was performed with two objectives. The first objective is to calibrate the numerical model, which, as explained in paragraph 3.2, involves microstructure aspects.

FEM SIMULATION

The aim of the numerical model is to simulate the thermal behavior of flawless welding, particularly the corresponding C1, C2, and C3 profiles for different welding parameter settings. These curves are validated by comparing them to corresponding experimental ones of sound

welding obtained with the same parameter setting. These simulated curves can then be used to assess the presence of defects by comparing them with actual experimental curves. Simulations were only run on SMAW butt weldings because the experimental validation of this preliminary investigation was more reliable in this configuration. The acquired surfaces are perpendicular to the IR sensor, and the thermal emissions are not affected by acquisition angles. The results will be extended to the T-joint and GMAW welding.

The CAD of the butt weld piece was modeled using Solidworks 2021. It is composed of an assembly of three bodies: two symmetrical plates of dimensions 500x125x5mm with a 20° V-shaped weld groove and the weld fill, which is defined as the group of elements of the whole filler contact body. The elements of the filler were set with mechanical and thermal scaled properties (Marc's option "quiet") by a factor of 10^{-5} before being activated by the moving thermal flux's volume. The simulation was performed using MSC Marc Mentat 2021 software. The model consists of 39,316 nodes and 123,620 Tetra4 elements (linear tetrahedral elements).

Figure 1 presents an overview of the meshed model. The constraints of the model were set on the two sides of the plate (purple arrow in Figure 1). The corresponding nodes' displacements and rotations in the x, y, and z-axis were constrained. The simulation is a coupled thermal and structural simulation. The analysed outputs of the simulation are: temperature data and phase volume fraction.

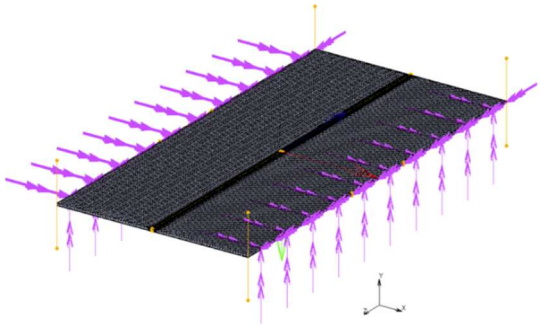

Fig. 1 – Meshed model.

RESULTS

In the experimental investigation, flaws such as suction pores, spatters, and breakthroughs were intentionally created in the welded joints. Burn-through, which is a trivial flaw to detect, was not presented in the results. Lack of penetration, which is difficult to detect in manual arc welding, was also considered, as it relates to a colder temperature of the weld pool. In this section, the results of both the experimental and numerical analyses will be presented. The aim is to identify the sound parameters for the welding process, which will then be used to validate the defect detection in section 4.4 by comparing the differences between sound (both simulated and experimental) and flawed curves

Experimental analysis

In Figure 2, we present two examples of C1 curves showing the temporal profile of four sound areas on the same butt welding with the same welding parameters. The results obtained from the reference area show a common pattern. The heating profile exhibits a noisy trend that can be attributed to various occurrences and phenomena, including the arc pass, IR reflection of the liquid weld pool, spatter, and fumes. Since manual welding is involved, obtaining repeatable and reliable thermal information from the weld pool area is challenging. However, this kind of artifact can be avoided in the case of automatic welding systems. Additionally, the extension of

the region of interest (ROI) during the heating step of the C1 curve, which is 3x3 pixels in this case, can affect the level of noise, and the single time-temperature curve may lose information on the generation of flaws in the welding pool, as the involved areas are larger than the 3x3 ROI. Moreover, the C1 cooling and heating profiles obtained experimentally are influenced by the position where the ROI is selected. For instance, an ROI at the beginning of the welding is surrounded by a volume of material whose temperature is lower than an ROI that is positioned in a subsequent place of the welding line, which reaches the highest temperature when the whole average temperature is higher. Generally speaking, the C1 time-temperature plot does not allow one to distinguish the different contributions of arc, weld pool, and fumes on the temperature plot.

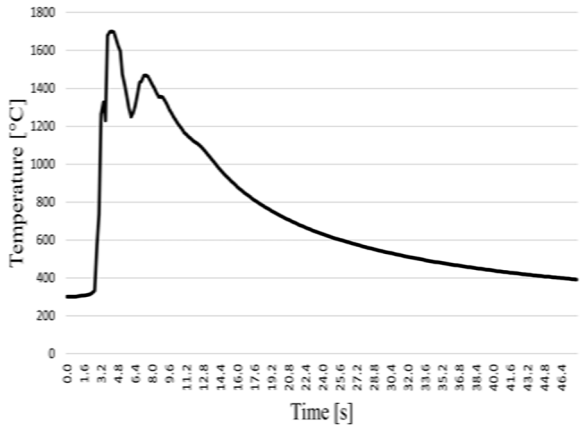

Fig. 2 – C1 curve in non-defect zone.

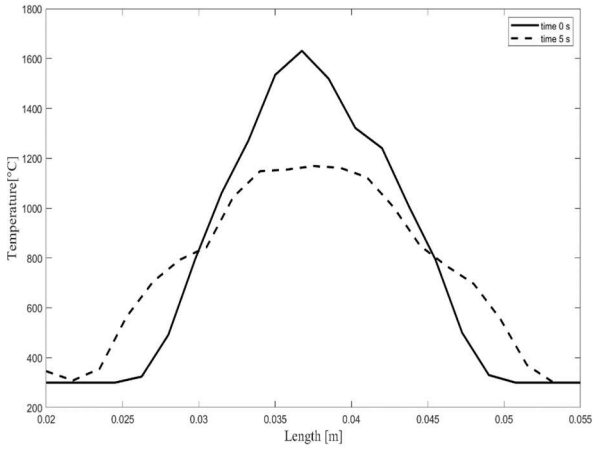

Fig. 3 – C3 curves at t=0s [-] and t=5s [- -] for sound butt SMAW joint.

The second common trend in the C1 curve consists in an almost constant temperature profile; it corresponds to the isothermal phase transition related to the solidification of the weld pool. After solidification, it can be recognized the typical exponential temperature decay which is a characteristic of thermal diffusive phenomena in bulk materials. This cooling profile presents no noise perturbation. The cooling curve gives an indication of the local quality of the joint, as will be later described. The C3 curves are important for analyzing the Heat Affected Zone (HAZ) and for calibrating the numerical simulation model. As shown in Figure 3, for a sound butt SMAW joint, as an example, the experimental temperature C3 curve presents a bell-shaped profile that tends to flatten after the weld torch passes the investigated ROI.

This curve represents how far from the weld path the heat diffuses, and the larger the C3 curve is, the larger the HAZ is. It is important to note that the shape of the C3 curve is affected by several factors such as the welding parameters, material properties, and geometry of the joint. The experimental data were used as input for the numerical simulation.

FE analysis

In figure 4, a comparison between the simulation results and the experimental acquisition is presented as an example. In particular, the C1 curves for sound regions are reported for butt welds. The simulated temperature curve reaches higher temperatures, and the constant temperature profile is not present. This is because the numerical solver is not able to simulate the phase transition corresponding to liquefaction and solidification (melting limit). Therefore, the numerical simulation heating flux, based on the Goldack model, continues to increment the temperature of the material. It should be noted that the numerical simulation can provide valuable information on the temperature distribution and evolution in the welded joint, which

is not always possible to obtain experimentally. However, it is important to validate the numerical model with experimental results to ensure its accuracy and reliability.

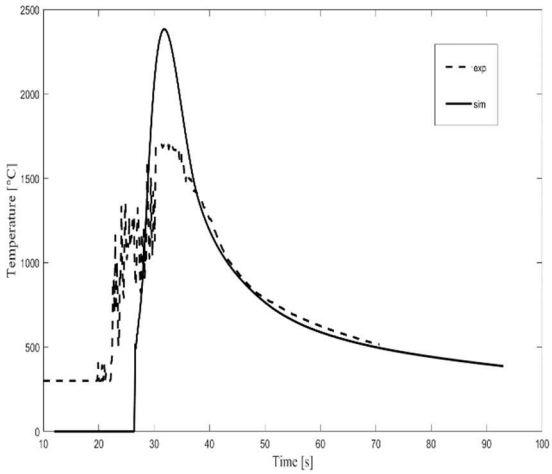

Fig.4 – C1 curves simulation [-] vs experimental [- -], butt joint SMAW weld.

The heating and cooling profiles in the numerical simulation show good agreement with experimental data, despite the presence of acquired experimental noise in the heating phase. The C1 curves obtained from the simulation can be used to calibrate the numerical model, for instance, by using the cooling profile to estimate the heat transmission rate. The validation of the model can be provided by comparing the C2 curves obtained from the simulation to the experimental data, as shown in Figure 5.

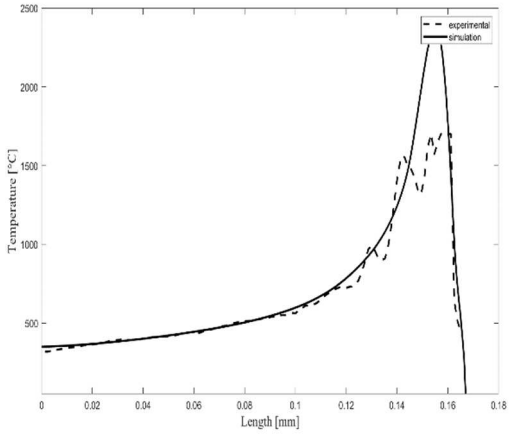

Fig. 5 – C2 curves simulation [-] vs experimental [- -].

The heating and cooling profiles in the numerical simulation show good agreement with experimental data, despite the presence of acquired experimental noise in the heating phase. The C1 curves obtained from the simulation can be used to calibrate the numerical model, for instance, by using the cooling profile to estimate the heat transmission rate. The validation of the model can be provided by comparing the C2 curves obtained from the simulation to the experimental data, as shown in figure 5. The C2 curves describe the heat transmission behavior of the material in front of and behind the heat flux during welding. The heat flow moves towards colder material, resulting in a steep pixel-temperature slope for the material in front of the heat front, while the material behind the heat front is warmer, resulting in a less steep pixel-

temperature slope. A careful calibration of the thermal physical constitutive model can provide a reliable simulation, as demonstrated in this case. The thermal diffusivity properties of the material are influenced by its phase distribution and microstructure, which must be taken into account during the calibration process. A reliable simulation can produce C2 and C3 curves that can provide information not only on the presence of flaws but also on HAZ extension and the actual phase composition in the welding.

Micrographic assessment

An additional parameter considered for the validation of the numerical model and for the determination of the quality of the joint is the HAZ dimension and composition. Then numerical and experimental results for sound weldings were compared.

The simulation of the micrographic composition provided as output in the weld bead a phases fraction, as presented in Table 2.

Tab.2 - Weld bead simulated phase fraction.

Martensite	Bainite	Pearlite	Ferrite
40%	50%	3%	7%

The visual inspection and image analysis of the microstructures in the welded zone, presented in Figure 9, allowed for the identification of mostly bainite and martensite in the microstructure, which is consistent with the simulation predictions. Both the Shielded Metal Arc Welding (SMAW) and Gas Metal Arc Welding (GMAW) methods exhibited similar microstructures in the weld bead, with slight differences in the transition zone. These differences could be attributed to the intrinsic differences in the welding processes and the variations in the consumable compositions, such as the cooling rate.

In terms of cooling rate, the slope of the C1 curves was used to calculate the cooling rate for the two different welding techniques, as reported in Table 3. The SMAW technique, which has a lower heat input, usually facilitates the generation of martensite.

Table 3 – Experimental cooling rate in sound butt welds.

Temperature	SMAW	GMAW
900°C	32 K/s	30 K/s
500°C	7 K/s	12 K/s

It can be observed that at 900°C, that is in the cooling interval after solidification and before phases nucleation, the two slopes are similar, while at 500°C, immediately before the martensite start temperature, the cooling rate in the SMAW technique is almost half of the GMAW one. This is an additional demonstration that the GMAW cooling transient, because of the lower heat input, leads to a higher martensite phase fraction.

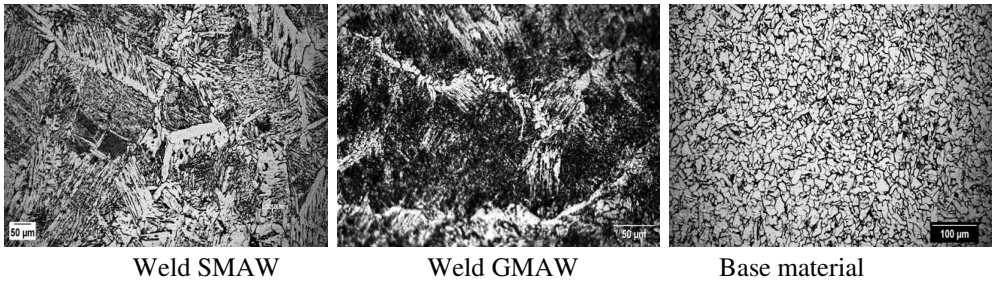

Weld SMAW Weld GMAW Base material

Fig. 6 – Weld microstructure.

Flaws detection

Both the experimental and numerical results provide insights into the expected thermal behavior of a defect-free welding process, based on the configuration of welding process parameters. The validation of the model and the proposed procedure is achieved by comparing the experimental C1, C2, and C3 curves of regions of interest (ROIs) where flaws were artificially introduced, with the corresponding simulated and/or experimental C1, C2, and C3 curves. As an example, in figure 10 (left), a C3 experimental curve corresponding to a suction pore (dotted line) is presented and compared to the C3 experimental curve of a sound region. The corresponding C2 curves are shown in Figure 7 (right). The temperature drop in the images indicates the presence of a defect. As demonstrated in Figures 7 and 8, the suction pore has a dimension similar to the electrode diameter, indicating that thermography can detect pores of at least a few millimeters in size.

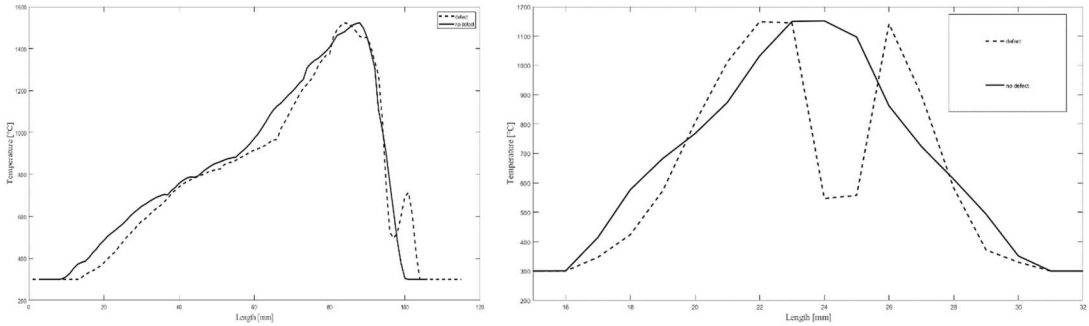

Fig. 7 – Sound [-] VS defective [- -] in C2 (left) and C3 (right) curves.

Another class of typical welding flaws is generated by arc instabilities. A non-stable arc generates improper fusion of the consumable electrode and bad penetration of the welding. This can be detected, for example, by analyzing the longitudinal profile, as shown in Figure 8. It can be observed that the thermal signal along the welding path is very noisy. There are lower temperatures and several colder temperature drops, while in the case of a correctly welded arc, the thermal profile shows a typical trend.

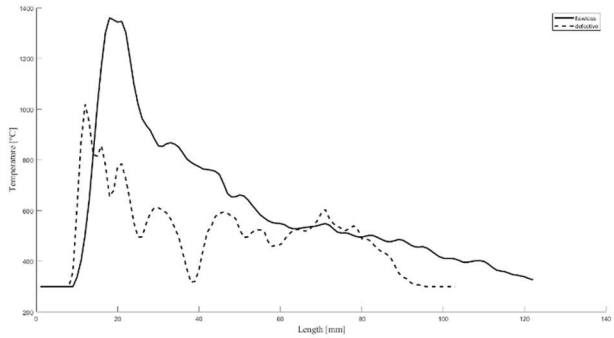

Fig. 8 – Wrong parameters effect on C2 curves, correct[-] VS unstable arc [- -].

This kind of flaws usually leads to lack of fusion defects and underfilling of the groove.

Given the validation of the experimental thermal curves for sound and flaw ROIs, then the simulations in different welding conditions can provide sound thermal contours to be compared with contours to be quality controlled.

CONCLUSIONS

In this work, we present a real-time analysis procedure for the welding process, joint HAZ extension, phase distribution, and flaw detection using thermographic analysis. Specifically, our proposed technique uses IR thermography for non-destructive evaluation of the weld pool, acquisition of the cooling transient, and thermal profiles of selected ROIs in low-carbon steel weldings. Our analysis focuses on subsurface defects, particularly suction pores.

It was implemented a numerical model of the welding process and corresponding heat-related phenomena to obtain thermal time and space plots in the joint surface based on the welding process parameter configuration. These simulations were calibrated using thermal acquisitions obtained during the welding process on sound butt and tee joints made of S275JR laminate steel plates.

Then it was compared the thermal profiles obtained on defective welded joints with simulated and experimental corresponding sound ones. This comparison revealed that mismatches in the profiles correspond to the presence of a flaw. We also extended our investigation to the analysis of artifacts in the thermal profiles to provide useful tools for interpreting the results.

It was compared the thermographic technique with other destructive methods, particularly for the estimation of the HAZ extension. We performed micrographic analysis to validate the experimental thermal profiles and simulation results. A good simulation with correct input parameters (thermo-physical and mechanical properties of the material) provides reliable space and time temperature curves that reproduce experimental behavior except for liquid to solid phase transition.

REFERENCES

[1] Ardika RD, Triyono T, Muhayat N, A review porosity in aluminum welding, Procedia Structural Integrity 33 (2021), pp.171-180.

[2] Filyakov AE, Sholokhov MA, Poloskov SI, Melnikov AY, The study of the influence of deviations of the arc energy parameters on the defects formation during automatic welding of pipelines, in: IOP Conference Series: Materials Science and Engineering, volume 966, 2020. doi: 10.1088/1757-899X/966/1/012088.

[3] Hong Y, Yang M, Chang B, Du D, Filter-PCA-Based Process Monitoring and Defect Identification During Climbing Helium Arc Welding Process Using DE-SVM, IEEE Transactions on Industrial Electronics (2022), pp.1343-1348.

[4] Nguyen HL, Van Nguyen A, Duy HL, Nguyen T-H, Tashiro S, Tanaka M, Relationship among Welding Defects with Convection and Material Flow Dynamic Considering Principal Forces in Plasma Arc Welding, Metals 11 (2021) 1444.

[5] Zhou Q, Rong Y, Shao X, Jiang P, Gao Z, Cao L, Optimization of laser brazing onto galvanized steel based on ensemble of metamodels, Journal of Intelligent Manufacturing 29 (2018), pp.1417-1431.

[6] Aucott L, Huang D, Dong HB, Wen SW, Marsden JA, Rack A, Cocks AC, Initiation and growth kinetics of solidification cracking during welding of steel, Scientific Reports 7 (2017).

[7] Hellinga MC, Huissoon JP, Kerr HW, Identifying weld pool dynamics for gas metal arc fillet welds, Science and Technology of Welding and Joining 4 (1999), pp.15-20.

[8] Alfaro SC, Franco FD, Exploring infrared sensoring for real time welding defects monitoring in GTAW, Sensors 10 (2010), pp.5962-5974.

[9] Yun TJ, Oh WB, Lee BR, Son JS, Kim IS, A study on the optimal offset distance between welding torch and the infrared thermometers, Fluid Dynamics and Materials Processing 15 (2019), pp.1-14.

[10] Naksuk N, Nakngoenthong J, Printrakoon W, Yuttawiriya R, Real-time temperature measurement using infrared thermography camera and effects on tensile strength and microhardness of hot wire plasma arc welding, Metals 10, (2020), pp.1-14.

[11] Speka M, Matteï S, Pilloz M, Ilie M, The infrared thermography control of the laser welding of amorphous polymers, NDT and E International 41 (2008), pp.178-183.

[12] Matteï S, Grevey D, Mathieu A, Kirchner L, Using infrared thermography in order to compare laser and hybrid (laser+MIG) welding processes, Optics and Laser Technology 41 (2009), pp.665-670.

[13] Cao Z, Yang Z, Chen XL, Three-dimensional simulation of transient GMA weld pool with free surface, Welding Journal (Miami, Fla) 83 (2004), pp.169-176.

[14] Zhu C, Cheon J, Tang X, Na SJ, Cui H, Molten pool behaviors and their influences on welding defects in narrow gap GMAW of 5083 Al-alloy, International Journal of Heat and Mass Transfer 126 (2018), pp.1206-1221.

[15] Cho DW, Na SJ, Cho MH, Lee JS, Simulations of weld pool dynamics in V-groove GTA and GMA welding, Welding in the World 57 (2013) pp.223-233.

[16] Sebayang D, Manurung YH, Ariri A, Yahya O, Wahyudi H, Sari AK, Romahadi D, Numerical simulation of distortion and phase transformation in laser welding process using MSC Marc/Mentat, in: IOP Conference Series: Materials Science and Engineering, volume 453, 2018. doi: 10.1088/1757-899X/453/1/012020.

[17] Ahmad SN, Manurung YH, Mat MF, Minggu Z, Jaffar A, Pruller S, Leitner M, FEM simulation procedure for distortion and residual stress analysis of wire arc additive manufacturing, in: IOP Conference Series: Materials Science and Engineering, volume 834, 2020. doi: 10.1088/1757-899X/834/1/012083.

[18] Arora H, Singh R, Singh Brar G, Thermal and structural modelling of arc welding processes: A literature review, Measurement and Control 52 (2019) pp.955-969.

[19] Meng X, Qin G, Su Y, Fu B, Ji Y, Numerical simulation of large spot laser + MIG arc brazing-fusion welding of Al alloy to galvanized steel, Journal of Materials Processing Technology 222 (2015), pp.307-314.